



Uphill Quenching to Reduce Residual Stress in Aluminium Alloy 7449 Hollow Structures

J. S. Robinson¹ · A. O' Donovan² · R. C. Wimpory³

Received: 24 January 2022 / Accepted: 4 March 2022 / Published online: 15 March 2022
© The Author(s) 2022

Abstract

Background Uphill quenching (UHQ) of heat treatable aluminium alloy components is a long established but rarely practiced or investigated method of reducing residual stresses. The efficacy of the technique has not been quantified on thin walled structures before and this investigation will address that deficiency.

Objective To quantify the impact of uphill quenching on thin walled structure with regards to residual stress and warpage, and compare and contrast to both quenching into cold water and a 30% polyalkylene glycol (PAG) solution.

Methods Rectilinear hollow boxes were made from the very high strength aerospace aluminium alloy 7449. These were heat treated and aged using a variety of processing methods including uphill quenching from -196 °C to 100 °C using steam. Residual stresses have been characterised using neutron and x-ray diffraction.

Results Compared to conventional quenching into cold water, both PAG and UHQ are shown to significantly lower the residual stresses. However, while PAG quenching results in a large uniform reduction in both residual stress and warpage, UHQ is much more localised and limited to regions adjacent to direct steam impingement. These regions are also warped. The depth of penetration of the stress relief during UHQ is shown to be 5 mm.

Conclusions While uphill quenching is shown to be capable of locally stress relieving an aluminium alloy, it is far less effective compared to PAG quenching.

Keywords Aluminium alloy 7449 · Heat treatment · Residual stress · Uphill quenching · Neutron diffraction

Introduction

Aluminium alloys find application in aerospace structures because they are heat treatable to medium to high strength levels. This combined with their low density has made them attractive for stiffness and strength critical applications in all types of aircraft since the birth of powered aviation. Their

Achilles heel is the relatively poor performance in fatigue, and their resistance to corrosion and stress corrosion. For these reasons, there has been a steady migration towards replacing aluminium alloys with composite materials since the 1980s [1–3]. The development of new and improved aluminium alloys has slowed as a consequence, but the availability, isotropy, manufacturing compatibility and well characterised performance means 2000 and 7000 series aluminium alloys remain important materials in aviation.

A key requirement of heat treatable alloys is the necessity to produce a supersaturated solid solution by rapid quenching. This can introduce warpage, cracking and distortion during subsequent machining operations [4–6]. In products with thick sections ($t > 15$ mm), residual stress magnitudes of ± 200 MPa are normal after rapid quenching from the solution heat treatment temperature [7]. For simple shapes, application of plastic deformation is used to reduce the residual stresses [8–11]. However, for complex shapes such as die forgings the extra expense of additional cold compression forging dies makes this uncommon [12]. Complex critical parts can be quenched less

✉ J. S. Robinson
Jeremy.robinson@ul.ie

A. O' Donovan
alan.odonovan@tus.ie

R. C. Wimpory
robert.wimpory@helmholtz-berlin.de

¹ School of Engineering, University of Limerick,
Limerick V94 T9PX, Ireland

² Department of Mechanical & Automobile Engineering, TUS,
Moylish Park, Limerick V94 EC5T, Ireland

³ Helmholtz-Zentrum Berlin Für Materialien Und Energie
GmbH, Hahn-Meitner-Platz 1, Berlin 14109, Germany



aggressively and the example of polyalkylene glycol (PAG) quenching is investigated here. An alternative technology is uphill quenching (UHQ) which reverses the thermal gradients encountered during quenching [13–16]. Uphill quenching can be applied to complex geometries that cannot be stress relieved economically by mechanical methods. Complex die forgings and castings are amenable. Limited data exists that fully quantifies the stress reduction process and how the distribution of residual stresses is changed through the thickness of components. Uphill quenching is labelled a “cryogenic or cold stabilisation” process but it should not be confused with the simple exposure of parts to sub-zero temperatures which has no effect. However, applying the rapid increase in temperature has limited the widespread application of UHQ. In addition, there is a logistical constraint of minimising the natural aging time between water quenching and immersion in the cryogenic fluid.

This experiment follows an investigation where solid blocks of the alloy 7449 were processed using conventional quenching and uphill quenching techniques [17]. Now similar blocks have been hollowed out to make boxes with variable wall thickness to assess residual stresses through the walls and warpage after quenching. The through thickness residual stress distribution has been characterised using neutron and X-ray diffraction. Both PAG quenching and uphill quenching in steam result in stress relief compared to cold water quenching. The effect of steam impingement is shown to be effective in lowering surface residual stress, but the effect is very localised, and the depth of penetration is shallow, confirming the earlier observations made on solid blocks.

Experimental Details

Materials and Sample Configuration

This experiment used six rectilinear hollow boxes made from the very high strength Al–Zn–Mg–Cu aerospace alloy 7449. The composition of the 7449 alloy is given in Table 1. Solid blocks of size 81 (x, Longitudinal) × 155 (y, Long Transverse) × 60 (z, Short Transverse) mm (mass 2.2 kg), were extracted from a section of a large, triaxially open die forged, rectilinear aircraft spar forging of dimension 3000 (L) × 160 (LT) × 126 (ST) mm. This parent forging was manufactured from a solid cylindrical cast ingot of 7449 alloy of mass 830 kg. The blocks were assumed chemically and mechanically homogeneous.

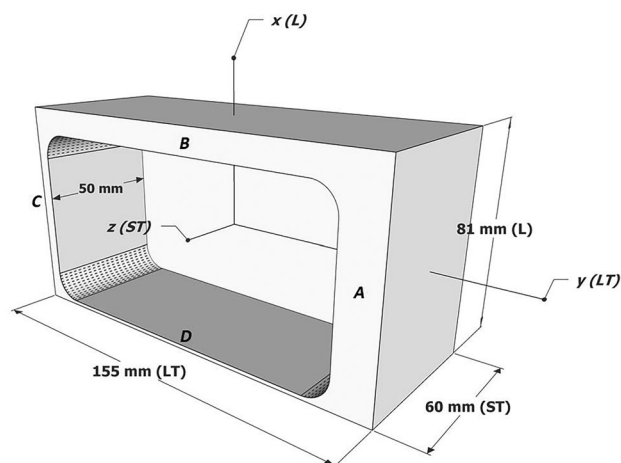


Fig. 1 The geometry of the hollow 7449 boxes. The base of the box was 10 mm thick. The side walls of the box were 15 (labelled A), 10 (B), 5 (C) or 1.5 (D) mm thick. The coordinate system defined in the figure was that used in the neutron diffraction measurements. Neutron diffraction measurements were made through the wall thickness in the centres of the walls for all but the 1.5 mm thick wall

The solid blocks were then machined to form the hollow boxes, an example of which is shown in Fig. 1. The wall thickness in the four walls of the box was varied from 15 to 1.5 mm. The base of the box was 10 mm thick. The fillet radius of the box corners was 10 mm. In one additional box, three 1.0 mm diameter type K shrouded thermocouples were inserted (parallel to the z or ST direction) in the centres of the 5, 10 and 15 mm walls to a depth consistent with the impingement area of the UHQ steam jets. These were to permit time temperature profiles to be determined during cold water, PAG and uphill quenching.

The optical microstructure of the parent forging when heat treated consisted of approximately rod shaped grains elongated into the longitudinal direction by the working operations, with a typical grain length being < 1000 μm. In the transverse directions, the grain characteristic dimension was < 200 μm. Within these grains a substructure was observed consisting of well-defined polygonised equiaxed sub-grains. The diameter of the sub-grains was < 20 μm. Other coarse phases noted were fragmented Al–Cu–Fe constituent particles and a very small volume fraction of undissolved MgZn₂. The material can be classified as unrecrystallised. The longitudinal 0.2% tensile proof stress of cold water quenched 7449 measured in small samples

Table 1 Specification alloy chemistry and chemical analysis (ca) results, wt%

Alloy	Si	Fe	Cu	Mn	Mg	Zn	Ti + Zr	Al
7449	0.12 max	0.15 max	1.4–2.1	0.20 max	1.8–2.7	7.5–8.7	0.25 max	Bal
7449 (ca)	0.06	0.08	2.02	0.01	1.92	8.39	0.138	Bal



immediately after cold water quenching is in the range 140 – 150 MPa.

Heat Treatment and Uphill Quenching

The normal precipitation hardening heat treatment for 7449 includes solution treating at 472 °C, followed by cold water (< 20 °C) immersion quenching and then (over) aging for 6 h at 120 °C + 10 h at 160 °C. All boxes were solution treated at 472 °C for 90 min. They were then quenched into cold water (< 20 °C) or a 30% (by volume) PAG solution so that the 15 mm thick wall entered the water (or PAG) first. The boxes were immersed rapidly, to ensure cooling was as uniform as possible. The cavity of the boxes filled as they were immersed in the quenchant and care was taken to ensure no vapour pockets formed. Two further boxes were then subject to uphill quenching. Each box was cooled to -196 °C in liquid nitrogen immediately after cold water quenching to minimise natural aging. As soon as a box equilibrated, it was placed into an aluminium alloy enclosure with four fixed nozzles connected to a 40 kW steam generator capable of delivering dry, or slightly superheated steam, at a nominal flow rate of 0.02 kg s⁻¹. Steam conditions could be varied from atmospheric (100 °C at 1 bar) to a maximum of 170 °C at 7 bar, depending on the circumstances. In this case, high velocity steam jets at slightly elevated atmospheric conditions were directed onto the centres of all four side walls. The duration of the uphill quench was 45–60 s. A complete typical thermal profile up to the end of the UHQ is shown in Fig. 2.

In summary, three conditions were examined, cold water quenched (CWQ) and aged, PAG quenched and aged and CWQ+UHQ (steam) and aged as shown in Table 2. The over-aging treatment lowers the as quenched residual stress magnitudes, but in 7449 with a maximum aging temperature of 160 °C, the influence is minor and results in a less than 30% reduction [18].

Thermal profiles during quenching were made using the box with three embedded thermocouples. Data was recorded at 25 Hz and multiple quenches were completed to assess repeatability.

Residual Stress Characterisation

Neutron Diffraction

Measurements were made following the guidelines present in recently published papers [19–21]. Neutron diffraction was performed on the strain scanning instrument, E3 (HZB, Berlin, Germany). This was used with monochromatic radiation of approximate wavelength 1.47 Å. The position of the {311} aluminium peak was determined. The sampling gauge volume was approximately 2 × 2 × X

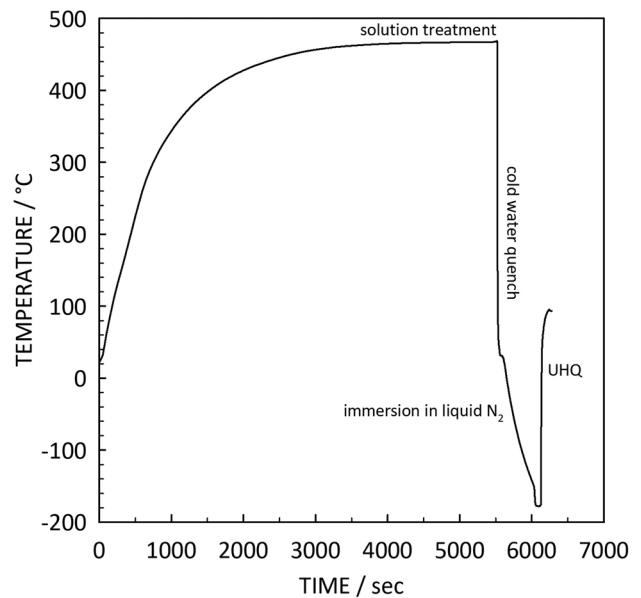


Fig. 2 Typical temperature time data including solution heat treatment at 472 °C, cold water quenching (T < 20 °C), immersion in liquid nitrogen (-196 °C) and uphill quenching in steam to ~ 100 °C

mm³ as defined by the incident beam slit width, the diffracted beam radial collimator and the slit height. The slit height X varied from 4 mm (number of grains estimated at 800) to 18 mm (1800 grains). The height of the gauge volume was varied to improve the counting statistics and reduce the uncertainties for certain line scans. The long dimension of the gauge volume was varied in a direction the strain was assumed to be relatively constant. The blocks were positioned on the instrument stage to permit measurements of strains in the three original primary working orthogonal directions as shown in Fig. 1. These directions were assumed to be the principal stress directions, being coincident with the direction of maximum heat flow out of the box wall surfaces during quenching.

Table 2 Heat treatment and fully heat-treated Vickers hardness measurements for the 7449 boxes. Artificial aging treatment was 6 h at 120 °C + 10 h at 160 °C

Block code	Quench	Strain free reference	Vickers hardness HV20
X10	Cold water (< 20 °C)		
X2	Cold water (< 20 °C)	✓ (for X10)	184 ± 3
X9	30% PAG (< 20 °C)		
X6	30% PAG (< 20 °C)	✓ (for X9)	178 ± 3
X5	CWQ+ Uphill quench		
X8	CWQ+ Uphill quench	✓ (for X5)	181 ± 4



The through thickness variation of residual stresses in the 5, 10 and 15 mm walls were determined. The number of measurement points was 5, 11 and 17 for the 5, 10 and 15 mm walls respectively, along a line coincident with a line with origin at the box centre, and normal to the wall surfaces. Measurements at the surface were duplicated where necessary, having rotated the boxes on the goniometer stage to permit correction for the gauge volume emerging from the sample. Each box also had a complimentary duplicate subject to the same processing as detailed in Table 2 to provide a strain free reference. Each wall was cut twice near its centre in the z direction by wire electro-discharge machining to produce a prism of material. These prisms of width 5 mm were left attached to the base of the box. Orthogonal measurements of strain were made in all the cut prisms through the thickness of the walls. In the event these strain free reference samples were not required as it was clear the walls were in a condition of plane stress. The neutron diffraction data is presented assuming the condition of plane stress; where the assumption is the stress in the wall thickness direction is zero.

Lattice spacings were converted to residual strains and stresses using the standard three dimensional Hooke's law [22]. A Young's modulus (E) of 70 GPa and a Poisson's ratio (ν) of 0.3 was used in all the calculations. These elastic constants have been found by the authors to offer the best agreement between neutron diffraction and other residual stress measurement techniques, including X-ray diffraction, incremental centre hole drilling and deep hole drilling for 7000 series alloys [23, 24]. Multiple (repeatability) neutron diffraction measurements on the blocks and the associated stress free samples allowed an estimation of one standard deviation random uncertainties as ± 30 MPa. These uncertainties were larger than the peak fitting errors. The microstructural induced variation along the length of the strain free reference was very small and encapsulated by the random uncertainties.

X-ray Diffraction

Surface residual stress measurements using a $\text{Sin}^2\psi$ technique were performed on a Panalytical X'Pert X-ray diffractometer using $\text{Cu K}\alpha$ radiation operating in the ω configuration. The measurement procedures followed best practice guidelines [25]. The position of the aluminium {422} peak was measured ($136^\circ < 2\theta < 139^\circ$). Sixteen scans were performed for each stress measurement using equally spaced ψ values within the range $0 \leq \psi \leq 60^\circ$ (positive tilting only, ψ -angle between the surface normal and the bisector of source and diffracted X-ray beam). The resulting spectra were analysed using Panalytical residual stress software (Version 2.3) with peak locations determined using a Pearson VII fitting technique. In all cases, the sixteen

peak positions were used to calculate the straight line d_{422} (interplanar spacing) versus $\text{Sin}^2\psi$ plots. The calculation of residual stress from the measured peak position was made using the established theory [26]. The elastic constants were taken from literature for the {422} planes [27]. The irradiated area was in the form of a line 2 mm wide and 12 mm long. The penetration depth of the X-rays was assumed to be of the order of 100 μm calculated using reference data [26]. Calibration of the diffractometer was performed using a specimen with a "known" residual stress. This specimen was a piece of cold water quenched and aged 7010 alloy that had been characterised on multiple neutron and X-ray diffractometers located in different institutions over a period of 20 years. The measurement locations were on the surface of the block on the perimeter of the quarter plane shown in Fig. 1. Where uncertainties are quoted, these are fit errors from the lattice spacing and $\text{Sin}^2\psi$ straight line plots.

Warpage Determination

An estimate of the warpage arising from quenching was determined by measuring the exterior surface profile of the 1.5 mm thick wall using a Hexagon GLOBAL Classic co-ordinate measuring machine (CMM). The surface was divided into a two-dimensional grid of 12×32 points with the displacement of each point determined relative to a datum plane defined by the constrained three adjoining walls.

Results

Cooling During Quenching

Figure 3 shows cooling rates developed during cold water quenching. The figure contains data for three quenches. The results were repeatable and consistent. The 5 mm thick wall (and by inference the 1.5 mm thick wall) cooled very rapidly with a maximum cooling rate of approximately $600 \text{ }^\circ\text{C s}^{-1}$ occurring when the thermocouple reported a temperature of $400 \text{ }^\circ\text{C}$. Maximum cooling rates in the other walls occurred at the same temperature and were approximately 400 and $200 \text{ }^\circ\text{C s}^{-1}$ for the 10 and 15 mm walls respectively. Aluminium alloy 7449 is not a quench sensitive alloy and this rapid cooling can be assumed to be more than sufficient to ensure the production of a supersaturated solid solution in all areas of the box.

Figure 4 shows the cooling rates during PAG quenching. The pattern of cooling was an initial period of rapid cooling upon immersion, followed by a reducing cooling rate as a viscous layer of PAG formed on the surface. A period of more rapid cooling then ensued as the gel like layer partially liquefied. The maximum cooling rate in the 5 mm



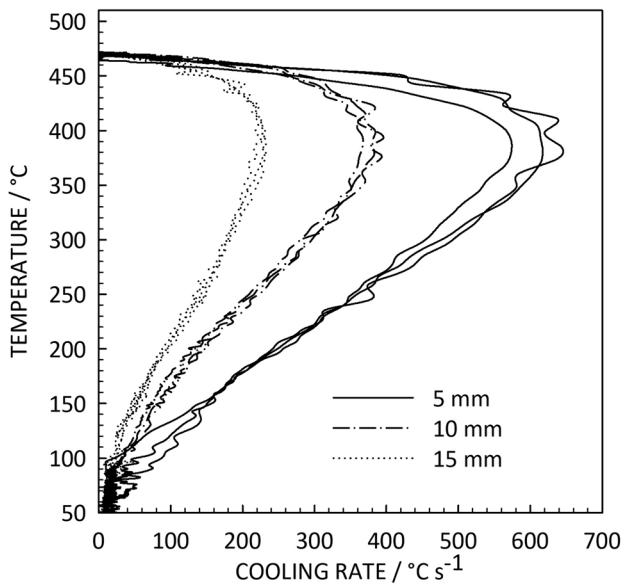


Fig. 3 Cooling rates during cold water quenching from 472 °C to room temperature at thermocouples located in the centres of the 5, 10 and 15 mm thick box walls. Cooling rates from three separate quenches are shown to illustrate the repeatability of the cold water quench for each wall thickness

wall was much lower (100 °C s^{-1} compared to 600 °C s^{-1}) when compared to cold water quenching and occurred at a much lower temperature. However, the impact of these reduced cooling rates on the subsequent aging response was

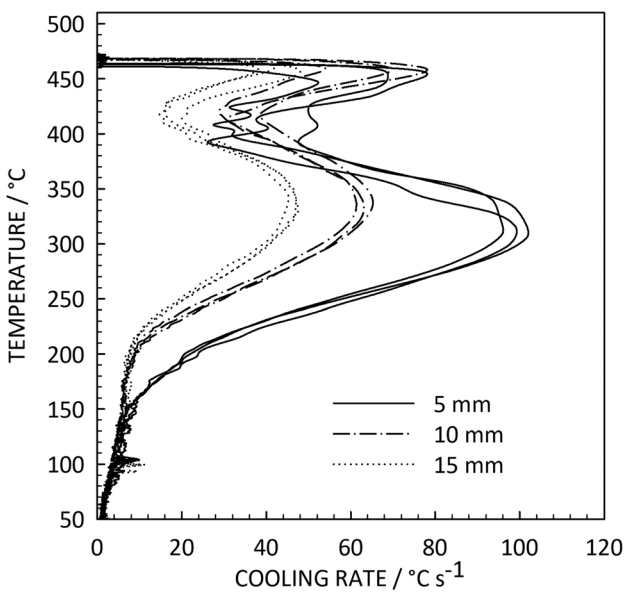


Fig. 4 Cooling rates during quenching into a 30% PAG solution from 472 °C to room temperature at thermocouples located in the centres of the 5, 10 and 15 mm thick box walls. Cooling rates from three separate quenches are shown which illustrates the repeatability of the PAG quench for each wall thickness. Note the different cooling rate axis range compared to Fig. 3

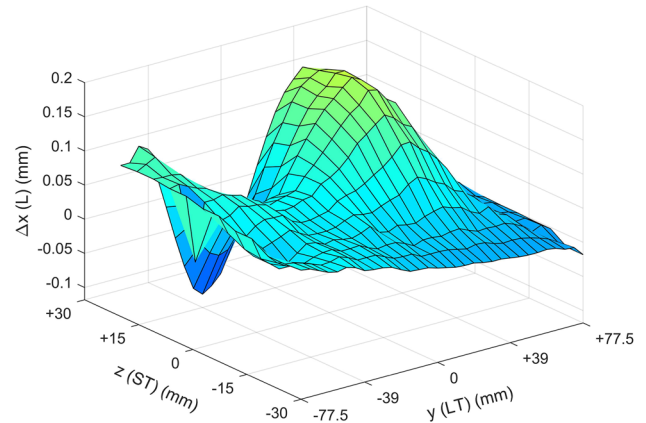


Fig. 5 Warpage of the 1.5 mm thick wall arising from rapid immersion in cold water after solution treatment at 472 °C. Coordinate system correspond to that defined Fig. 1. $z = +30\text{ mm}$ corresponds to the free edge of the wall. $y = +77.5$ corresponds to the outer edge of the 15 mm thick wall, and -77.5 mm is the 5 mm wall. The 15 mm thick wall entered the quench first

very small and the indentation hardness of the PAG box material was almost identical to cold water quenched, see Table 2. The 0.2% proof stress of fully heat treated PAG and CWQ material measured in round bar tensile test samples of 12.5 mm diameter were both $502 \pm 2\text{ MPa}$. The tensile strength (540 MPa) and elongation at fracture (10%) were also within experimental uncertainty.

During uphill quenching, the walls of the boxes increased in temperature from approximately -190 °C to 100 °C . The time taken for this temperature rise was approximately 10, 14 and 15 s for the 5, 10 and 15 mm thick walls respectively.

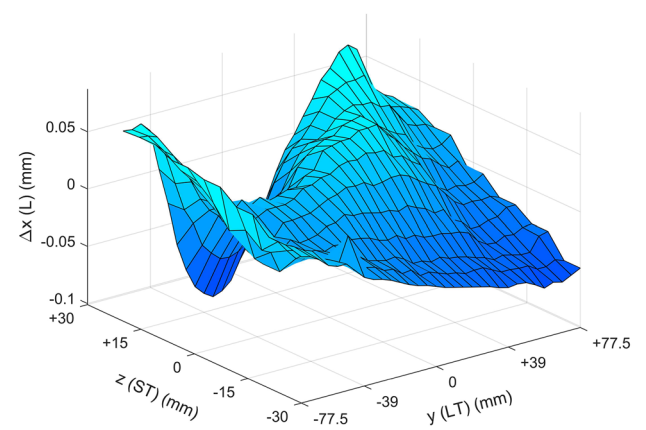


Fig. 6 Warpage of the 1.5 mm thick wall arising from rapid immersion in PAG after solution treatment at 472 °C. Coordinate system correspond to that defined Fig. 1. $z = +30\text{ mm}$ corresponds to the free edge of the wall. $y = +77.5$ corresponds to the outer edge of the 15 mm thick wall, and -77.5 mm is the 5 mm wall. The 15 mm thick wall entered the quench first



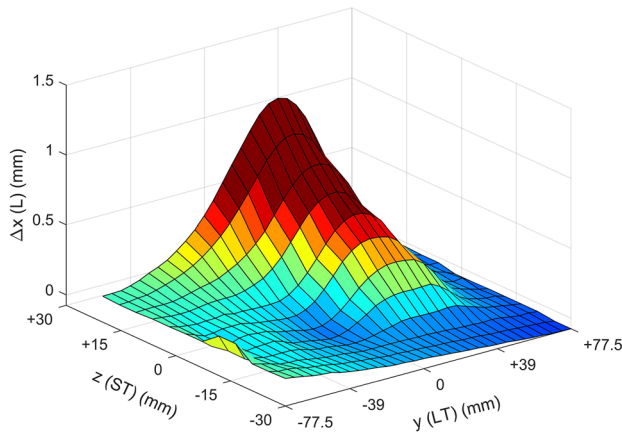


Fig. 7 Warpage of the 1.5 mm thick wall arising from cold water quenching after solution treatment at 472 °C, immersion in liquid nitrogen and then uphill quenching in steam. Coordinate system correspond to that defined Fig. 1. $z=+30$ mm corresponds to the free edge of the wall. $y=+77.5$ corresponds to the outer edge of the 15 mm thick wall, and -77.5 mm is the 5 mm wall. The 15 mm thick wall entered the quench first

Warpage During Quenching

The warp in the 1.5 mm wall of the CWQ box is shown in Fig. 5. The maximum warp in the wall was 0.19 mm and occurred towards the free edge of the 1.5 mm thick wall (as opposed to the area of the wall constrained by the base of the box). This was an outward bulge in the wall. Relative to the wall thickness this is a warpage of 13%. The total warpage of the wall including inward distortion was 0.31 mm or 21%. The maximum warpage was adjacent to the 15 mm thick wall which entered the quench first (see Fig. 6).

PAG quenching is known to reduce the warp arising from rapid cooling. The maximum warp was 0.09 mm or 6%. The pattern of warpage was the same the cold water quenched

box, with the maximum warp occurring adjacent to the 15 mm thick wall. The total warpage of the wall including inward distortion was 0.19 mm or 13%.

The uphill quenched box was not measured for distortion before being subject to the steam, as the uphill process had to be completed as soon as possible after cold water quenching from 472 °C. It is assumed the initial pattern of warpage would be similar to that shown in Fig. 5. The final warpage in the box after the UHQ is shown in Fig. 7. It can be seen there is a significant outward bulge located in the area subject to the steam impingement. The maximum warp was 1.19 mm or 79% of the wall thickness. The total warpage of the wall, including a very small inward distortion was 1.26 mm or 84%. These numbers are based on the box dimensions before the initial cold water quench.

Residual Stress Measurements

Cold Water Quenched Boxes

Cooling from the solution heat treatment temperature by immersion quenching is rapid, as has been shown above, and it is the thermal gradients from surface to interior that cause inhomogeneous plastic flow which in turn give rise to residual stress. The magnitude of these residual stresses through the thickness of the box walls quenched into cold water are shown in Fig. 8. As expected, the surface residual stresses were compressive on the exterior surfaces with the interior surfaces bordering the internal cavity being less. This will be a consequence of a slower rate of cooling for the internal wall surfaces. The residual stress magnitudes diminished with wall thickness. The residual stresses at the surface were predominantly equibiaxial, as shown in Fig. 9. However, in the 1.5 mm wall an anomalous result was recorded for the σ_{yy} component (-108 ± 7 MPa) compared to the σ_{zz} component (-26 ± 14 MPa). This was the only wall

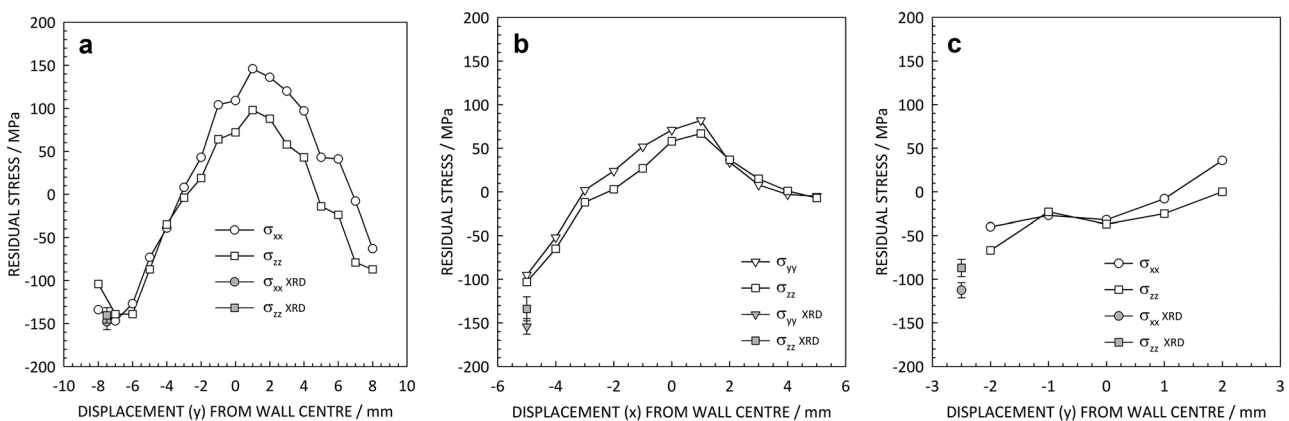


Fig. 8 Through thickness residual stresses in the 15 mm (a), 10 mm (b) and 5 mm (c) walls of the cold water quenched box. Neutron diffraction and x-ray diffraction results



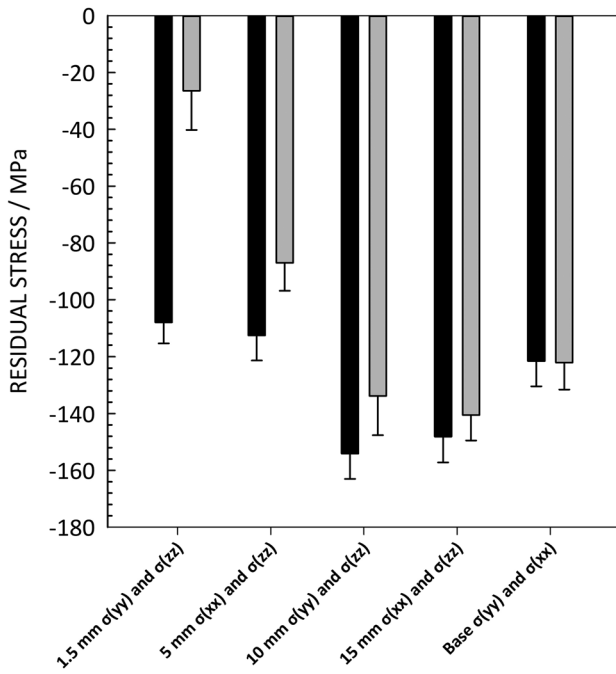


Fig. 9 Surface residual stresses measure in the cold water quenched box wall surfaces by x-ray diffraction

to suffer observable warpage under all quenching conditions. A 1.5 mm wall was wire cut from an additional box and heat treated. When the wall was unconstrained during quenching, the surface residual stresses reverted to equibiaxial of magnitude -60 MPa, suggesting a compressive stress arising from the warpage was influencing the measurement of the 1.5 mm box wall.

PAG Quenched Boxes

Figure 10 illustrates the through thickness residual stresses in the box quenched into the 30% PAG solution. It is clear

that quenching into PAG has had a dramatic influence on the residual stress magnitudes compared to CWQ. All three walls of the box are almost free of residual stress. Like the CWQ box, the 1.5 mm wall surface did have a large residual stress in the y (LT) direction ($\sigma_{yy} = -87 \pm 4$ MPa) as shown in Fig. 11. The same sectioning process was undertaken, and in the unconstrained wall, the residual stress became equibiaxial of magnitude -18 ± 2 MPa.

UHQ Quenched Boxes

The residual stresses remaining in the walls after UHQ are shown in Fig. 12. In the 15 mm thick wall the distribution of the residual stresses is similar to CWQ apart from a significant reduction adjacent to the point of steam impingement. The depth of stress relief was of the order of 5 mm. A similar reduction was noted in the 10 mm and 5 mm thick walls which confirms the UHQ is effective at stress relieving to a significant depth. Figure 13 shows the surface residual stresses in the walls. In this figure it is obvious the stress relief from UHQ can be non-uniform as indicated by the larger σ_{zz} component in the 10 mm wall. It can also be noted in this figure that despite the base of the box being exposed to the steam indirectly, there is very little, if any stress relief.

Discussion

Comparing Fig. 8 to Fig. 9 clearly demonstrates why PAG quenching has become so dominant when heat treating aluminium alloys for parts where residual stresses, warpage or subsequent distortion must be minimised. Quenching into PAG, for the geometry investigated here, renders the box almost residual stress free. The only caveat is the residual stress present in the long direction of thin wall which in the PAG case is insufficient to

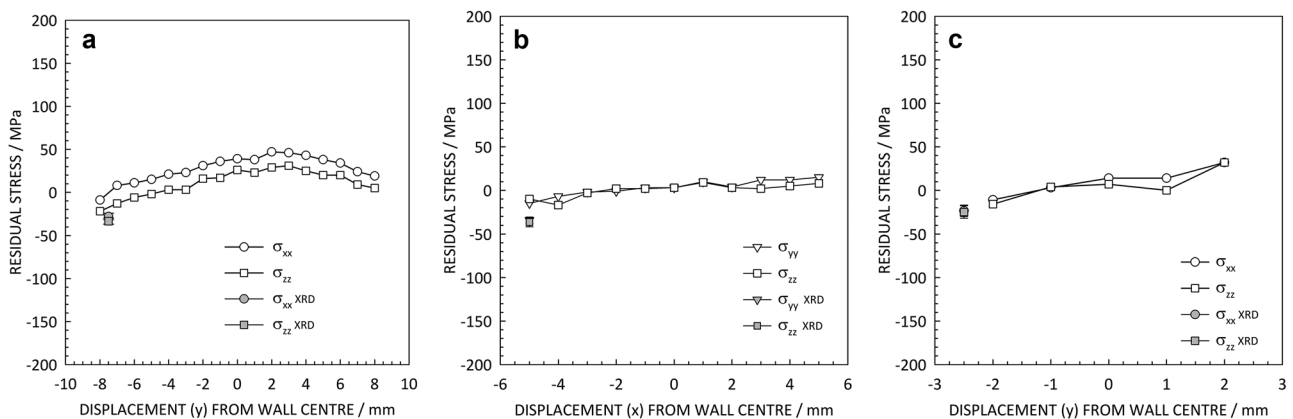


Fig. 10 Through thickness residual stresses in the 15 mm (a), 10 mm (b) and 5 mm (c) walls of a box quenched into a 30% PAG solution. Neutron diffraction and x-ray diffraction results



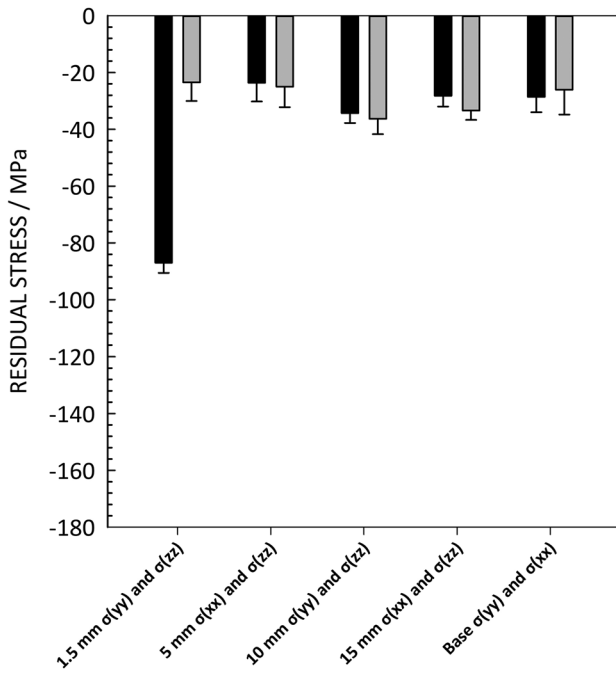


Fig. 11 Surface residual stresses measure in the PAG quenched box wall surfaces by x-ray diffraction

buckle the wall significantly. PAG works by slowing the cooling rate, especially around 400 °C (Fig. 4) where the alloy is very soft. (10–20% of the strength of the alloy at room temperature) [17]. Slower cooling can influence mechanical properties, but modern 7000 series alloy

including 7449, are not regarded as a quench sensitive and for this box geometry, there was no significant difference in hardness and strength. PAG quenching does come with an environmental cost as the quenchant must be disposed of appropriately after use, and the gel can contaminate the surface of the parts, so additional cleaning of the parts may be required. Uphill quenching could be argued to be more environmentally friendly than PAG quenching, only requiring the energy required to create plentiful steam. However, based on the observations here, it is unlikely there is going to be a rush to replace PAG with such a procedure. UHQ does work effectively, but it relies on direct steam impingement. This is its main limitation, and is what has limited its more widespread application from when it was first investigated many years ago. The necessity to construct bespoke steam chambers with a multiplicity of nozzles ensuring all surfaces are exposed to the steam is too onerous and potentially expensive. If the depth of stress relief was significantly greater than the 5 mm observed here, then it could be attractive for parts where PAG quenching might result in too great a loss of mechanical properties, in the fully heat treated part. It remains to be seen if increasing the intensity of the uphill quench can achieve a greater depth of stress relief. In summary, UHQ is a technology where the window of opportunity has probably now closed, except for limited niche applications. PAG quenching and the continuing replacement of aluminium alloys components with those made from polymer composites have inhibited its more widespread adoption.

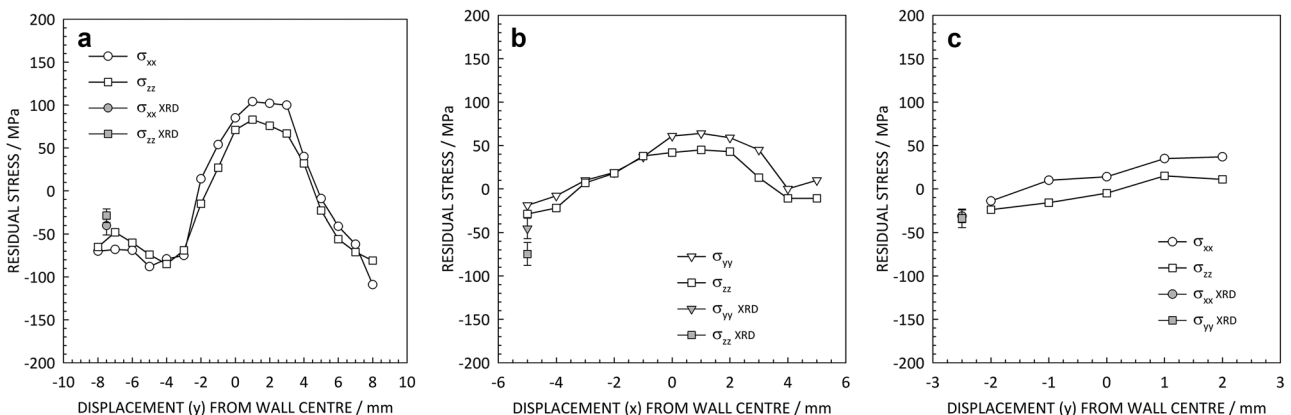


Fig. 12 Through thickness residual stresses in the 15 mm (a), 10 mm (b) and 5 mm (c) walls of a box quenched into a cold water and then subjected to UHQ. Neutron diffraction and x-ray diffraction results



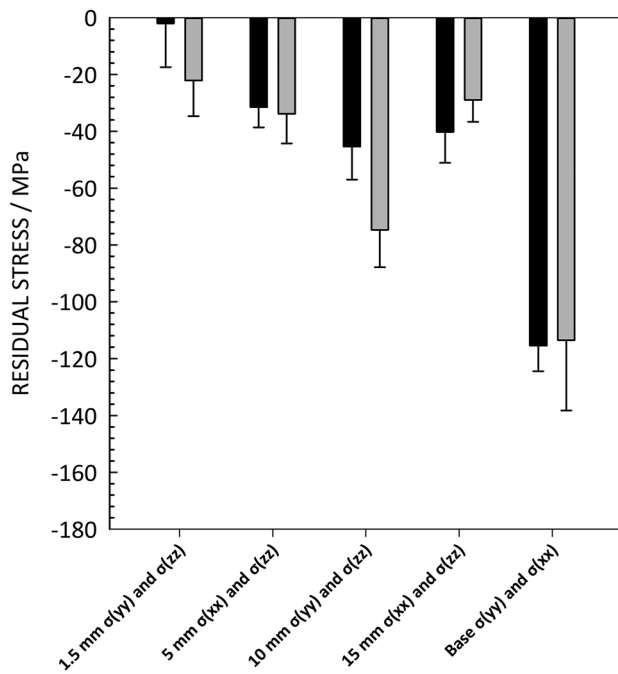


Fig. 13 Surface residual stresses measure in the UHQ box wall surfaces by x-ray diffraction

Conclusions

1. Uphill quenching and PAG quenching have both demonstrated the potential to lower residual stress introduced during the quenching stage of the heat treatable aluminium alloy 7449.
2. Quenching the boxes investigated here into PAG results in an almost completely residual stress free structure, with very little warpage of the thinnest wall compared to the cold water quenched box.
3. Uphill quenching into steam at 100 °C caused rapid heating of the material adjacent to the steam jet. At these locations, the residual stress was completely relaxed. The effect was localised, and other surfaces only demonstrated very minor stress relief.
4. The depth of penetration of the stress relief in the UHQ box under the steam jet was approximately 5 mm which is the same as the depth of relief observed in solid blocks of 7449.
5. The area of the thinnest wall subject to direct steam impingement suffered severe warpage.

Acknowledgements The authors are grateful for the neutron beam time provided by the HZB on the E3 instrument (experiment 191-07899).

Funding Open Access funding provided by the IReL Consortium.

Declarations

Conflict of Interest No potential conflict of interest was reported by the authors.

Open Access This article is licensed under a Creative Commons Attribution 4.0 International License, which permits use, sharing, adaptation, distribution and reproduction in any medium or format, as long as you give appropriate credit to the original author(s) and the source, provide a link to the Creative Commons licence, and indicate if changes were made. The images or other third party material in this article are included in the article's Creative Commons licence, unless indicated otherwise in a credit line to the material. If material is not included in the article's Creative Commons licence and your intended use is not permitted by statutory regulation or exceeds the permitted use, you will need to obtain permission directly from the copyright holder. To view a copy of this licence, visit <http://creativecommons.org/licenses/by/4.0/>.

References

1. Polmear I et al (2017) 2 - Physical metallurgy of aluminium alloys. In: Polmear I et al (eds) Light alloys, 5th edn. Butterworth-Heinemann, Boston, pp 31–107
2. Jayakrishna K et al (2018) 1 - Materials selection for aerospace components. In: Jawaid M, Thariq M (eds) Sustainable composites for aerospace applications. Woodhead Publishing, pp 1–18
3. Charles JA, Crane FAA, Furness JAG (1997) 15 - Materials for airframes. In: Charles JA, Crane FAA, Furness JAG (eds) Selection and use of engineering materials, 3rd edn. Butterworth-Heinemann, Oxford, pp 227–255
4. Mena R et al (2020) Distortions in large aluminum forgings: current situation and simulation challenges. In: Computation and big data for transport
5. Aurrekoetxea M, López de Lacalle LN, Llanos I (2020) Machining stresses and initial geometry on bulk residual stresses characterization by on-machine layer removal. *Materials* 13(6):1445
6. Masoudi S et al (2015) The effect of quench-induced residual stresses on the distortion of machined thin-walled parts. *J Mater Eng Perform* 24:3933–3941
7. Lin GY et al (2003) Residual stress in quenched 7075 aluminum alloy thick plates. *Tran Nonferrous Met Soc Chin* 13(3):641–644
8. Myer RT, Kilpatrick SA, Backus WE (1959) Stress-relief of aluminium for aircraft. *Met Prog* 3:112–115
9. Kleint RE, Janney FG (1958) Stress relief in aluminum forgings. *Light Met Age* 2:14–21
10. Klein J (1967) Cold reduction technique puts more forgings in the air. *Prec Met Mold* 6:53–54
11. Betteridge W (1948) The relief of internal stresses in Aluminum alloys by cold working. In: Symposium on internal stresses in metals and alloys. Institute of Metals, London
12. Nickola WE (1988) Residual stress alterations via cold rolling and stretching of an aluminum alloy. *ASTM STP* 993:7–18
13. International S (2013) AMS2767 Uphill Quenching of Aluminum Alloy Product. SAE International.
14. Hill HM, Barker RS, Willey LA (1959) The thermal mechanical method for relieving residual quench stresses in aluminum alloys. *Trans Am Soc Met* 52:657–671
15. Mattos WS, Totten GE, Canale LCF (2017) Uphill Quenching of Aluminum Alloys. *Mater Perform Charact* 6(5):894–903



16. Lados DA, Apelia D, Wang LB (2010) Minimization of residual stress in heat-treated Al-Si-Mg cast alloys using uphill quenching: Mechanisms and effects on static and dynamic properties. *Mater Sci Eng A Struct Mater* 527(13–14):3159–3165
 17. Robinson JS et al (2019) Uphill quenching to reduce residual stress in a heat treatable aluminium alloy. *Mater Sci Technol* 35(15):1864–1871
 18. Robinson JS et al (2012) Influence of quenching and aging on residual stress in Al-Zn-Mg-Cu alloy 7449. *Mater Sci Technol* 28(4):420–430
 19. Krawitz AD (2011) Neutron strain measurement. *Mater. Sci Technol* 27(3):589–603
 20. 21432, DCIT (2005) Non-destructive testing. Standard test method for determining of residual stresses by neutron diffraction. British Standards Institute, London
 21. ISO/TTA3, Ohms C, Youtsos AG, Webster GA, Wimpory RW (2001) Polycrystalline materials – Determination of residual stresses by neutron diffraction. In: Technology trends assessment. International standardisation organisation
 22. Hutchings MT et al (2005) Introduction to the characterisation of residual stress by neutron diffraction. CRC Press, Boca Raton, FL, USA, p 424
 23. Robinson JS et al (2015) Residual stress relief in the aluminium alloy 7075. in MECA SENS VIII 8th International conference on mechanical stress evaluation by neutron & synchrotron radiation. Grenoble, France: Trans Tech
 24. Robinson JS et al (2009) Influence of cold compression on the residual stresses in 7449 forgings. *Adv X-ray Anal* 52:667–674
 25. Fitzpatrick ME et al (2002) Determination of residual stresses by X-ray diffraction. Measurement Good Practice Guide. NPL
 26. Cullity BD, Stock SR (2001) Elements of x-ray diffraction, 3rd edn. Prentice Hall, Upper Saddle River, New Jersey, USA
 27. Hauk VM, Macherauch E (1983) A useful guide for X-ray stress evaluation (XSE). *Adv X-ray Anal* 27:81–89
- Publisher's Note** Springer Nature remains neutral with regard to jurisdictional claims in published maps and institutional affiliations.

